

# Proposal for a Mechanical Model of Mobile Shales

Juan Soto ([✉ juan.soto@beg.utexas.edu](mailto:juan.soto@beg.utexas.edu))

Bureau of Economic Geology (The University of Texas at Austin)

Mahdi Heidari

Bureau of Economic Geology (The University of Texas at Austin)

Michael Hudec

Bureau of Economic Geology (The University of Texas at Austin)

---

## Research Article

**Keywords:** mobile shale, continental margins

**Posted Date:** June 3rd, 2021

**DOI:** <https://doi.org/10.21203/rs.3.rs-537378/v2>

**License:**  This work is licensed under a Creative Commons Attribution 4.0 International License.

[Read Full License](#)

---

**Version of Record:** A version of this preprint was published at Scientific Reports on December 1st, 2021.

See the published version at <https://doi.org/10.1038/s41598-021-02868-x>.

# **PROPOSAL FOR A MECHANICAL MODEL OF MOBILE SHALES**

**Juan I. Soto<sup>(1,2) (\*)</sup>, Mahdi Heidari<sup>(1)</sup>, and Michael R. Hudec<sup>(1)</sup>**

(1) Bureau of Economic Geology, Jackson School of Geosciences, The University of Texas at Austin, University Station, Box X, Austin, Texas, 78713-8924, USA

(2) On leave of absence from: Departamento de Geodinámica, Universidad de Granada, Avenida de Fuente Nueva s/n, 18071 Granada, Spain

(\*) Corresponding author: juan.soto@beg.utexas.edu

1 Structural systems involving mobile shale represent one of the most difficult challenges for  
2 geoscientists dedicated to exploring the subsurface structure of continental margins. Mobile-  
3 shale structures range from surficial mud volcanoes to deeply buried shale diapirs and shale-  
4 cored folds. Where mobile shales occur, seismic imaging is typically poor, drilling is hazardous,  
5 and established principles to guide interpretation are few. The central problem leading to these  
6 issues is the poor understanding of the mechanical behaviour of mobile shales. Here we propose  
7 that mobile shales are at critical state, and discuss how this proposition can explain key  
8 observations associated with mobile shales. The critical-state model can explain the occurrence  
9 of both fluidized shales (e.g., in mud volcanoes) and more viscous shales flowing with grain-to-  
10 grain contact (e.g., in mud diapirs), mobilization of cemented or compacted materials, and the  
11 role of overpressure in shale mobility. Our model offers new avenues for understanding complex  
12 and fascinating mobile-shale structures.

13 Mobile shales are bodies of highly sheared shale that lack coherent reflections in seismic  
14 images. Mobile-shale structures range from surficial mud volcanoes to deeply buried shale  
15 diapirs and shale-cored folds (Fig. 1a–e). Although they exist in all tectonic regimes (Fig. 1f),  
16 they are mostly found in shortening settings (40%) or delta systems on continental margins  
17 (31%) (detailed information in Supplementary Discussion 1).

18 Mobile shales create challenges for seismic processing, seismic interpretation, drilling, and  
19 geohazards analysis. A primary source of uncertainty in interpreting these structures is a poor  
20 understanding of the mechanics of mobile shale. Although mobile shales appear to deform  
21 through some sort of ductile flow<sup>1–3</sup>, we have little insight into what can make shales flow. Most  
22 authors suggest that shales become mobile simply by becoming highly overpressured<sup>4–5</sup>,  
23 although this simple model fails to account for the full range of mobile-shale occurrence. For  
24 example, shales (defined broadly, *sensu* Aplin et al.<sup>6</sup>) can apparently become mobile even after  
25 significant burial, consolidation, and cementation<sup>7–8</sup>. Overpressure can mobilize unconsolidated  
26 mud, but an increase in pore pressure alone cannot cause a cemented shale to flow.

27 Our lack of a viable mechanical model for mobile shale is due partly to the difficulty in sampling  
28 subsurface mobile shales. Although mud volcanoes have been extensively studied<sup>9–13</sup>, little  
29 progress has been made in studying plastic flow of mobile shales using sampling  
30 observations<sup>2,14–17</sup> or drilling data<sup>18–19</sup>. As a result, we have little knowledge of the physical  
31 properties of plastically flowing shales in the subsurface and even less knowledge of the  
32 mechanical processes by which they become mobile or stop moving.

33 This uncertain understanding is reflected in the existing definition of *mobile shale*. The term was  
34 introduced by Morley and Guerin<sup>1</sup>, who defined them as “any shales deforming complexly by a

35 combination of ductile deformation and brittle failure in the presence of a fluid phase.” This  
36 definition was an excellent starting point because it recognized the roles of lithology,  
37 deformation style, and fluids in shale mobility. However, it suffers from several shortcomings.  
38 First, the definition is overly broad because it includes almost any type of deformation involving  
39 shales. Second, it provides little insight into what makes a mobile shale mobile or how it  
40 deforms.

41 In this paper, we summarize observations concerning mobile shales, and then propose a  
42 mechanical model that can explain these observations. We explore the implications of this model  
43 and its answers to key questions in mobile-shale research: How do shales become mobile? Is  
44 deformation in mobile shales brittle, ductile, or both? Why do some mobile shales become  
45 immobile? Can shales with diagenetic cements become mobile? Does depth of burial play a role  
46 in shale mobilization? Do all mobile shales have to be highly overpressured? If so, how high  
47 must the overpressure be? How does shale mobilization affect its seismic properties?

48

## 49 **What do we know about the mechanics of mobile shales?**

50 There are some observations about mobile shales that are widely accepted. We use these  
51 observations as a framework to suggest a mechanical model for mobile shales.  
52 First, there are two distinct types of mobile-shale structures<sup>3</sup>. The first occurs when the shale  
53 behaves as a fluid suspension without grain-to-grain contact<sup>20-21</sup>. Because of their low viscosity,  
54 this type of mobile shales forms smaller features like mud volcanoes (Fig. 1a–b) in which the  
55 shale moves at high velocities (up to tens of meters per second)<sup>11–13,22</sup>. In the second type, shale  
56 behaves as a viscous-plastic solid involving grain-to-grain frictional flow<sup>2</sup> or creep<sup>23</sup>. Because of

57 their high viscosity, this type of mobile shale forms large-scale bodies like shale diapirs (Fig.  
58 1c–e) that move at lower velocity than in mud volcanoes.

59 Second, bedding and other fabrics in mobile-shale structures are strongly disrupted, recording  
60 large and extensive shear deformation. This disruption is one factor causing the loss of seismic  
61 signal in mobile shale (Fig. 1c–e)<sup>24,25</sup>.

62 Third, mobile shales are typically associated with high overpressures. Overpressure is obvious in  
63 the fluidized material erupted from mud volcanoes, where there is almost no contact between  
64 grains<sup>9,10,11,13,14</sup>. High overpressure in other types of mobile shales such as shale diapirs can be  
65 inferred from the low seismic velocities of these bodies<sup>1,3,18,24,26</sup>. Most researchers attribute these  
66 overpressures to a combination of increase in the volume of the pore fluid (due to, e.g.,  
67 hydrocarbon generation and cracking, diagenetic transformations, or thermal expansion) and in  
68 total compressive stresses<sup>27</sup>. For example, based on the abundance of methane expelled during  
69 mud-volcano eruptions<sup>9-14,22</sup>, the mobility of shale in mud volcanoes is attributed to hydrocarbon  
70 transformations and the depressurization of a gas-charged source layer.

71 Fourth, given the stratigraphic position of blocks ejected from mud volcanoes, some mobile  
72 shales are sourced from depths of 9 to 10 km<sup>11,13,22,28-30</sup> (detailed information in Supplementary  
73 Discussion 1). Units sourced from these depths were cemented prior to incorporation in mud  
74 volcanoes. This observation represents a challenge for workers in mobile shales, because it is  
75 difficult to explain how these cemented blocks were mobilized.

76 Any viable mechanical model for mobile shales must be able to explain and be consistent with  
77 these observations: fluidization and plastic flow of shales, disruption of fabrics, existence of high  
78 overpressure, and mobilization of cemented units.

79

80 **Mechanical model for mobile shales: deformation at the critical state**

81 As mentioned earlier, field observations of subsurface mobile shales are scarce owing to the  
82 understandable reluctance of drillers to penetrate them. We therefore turn to experimental  
83 deformation of shales, to examine whether they provide any explanation for mobile-shale  
84 behaviour. Because these tests are typically conducted at low stresses and on poorly lithified  
85 soils, they do not directly mimic subsurface conditions. The principles governing the mechanical  
86 behaviour of soils<sup>31–32</sup> have also been used to analysed the behaviour of consolidated shales,  
87 although important differences exist between the mechanical behaviour of soils and shales<sup>33–35</sup>.  
88 According to these studies, shales differ from soils in that they have a major cohesion (stiffness),  
89 develop some degree of cementation and anisotropy, and their mechanical characteristics change  
90 with depth and temperature (detailed information in Supplementary Discussion 2, Table s2 and  
91 Fig. s4). Principles of soil mechanics have also begun to be extrapolated to depths at which  
92 diagenetic transformations operate in shales so that the mechanical behaviour of cemented shales  
93 deformed under contraction might be modeled<sup>36–38</sup>.

94 We use the behaviour observed in laboratory tests to infer the mechanical behaviour of mobile  
95 shales. Figure 2 illustrates the stress paths and the stress-strain response obtained from undrained  
96 triaxial tests on Norrköping clays<sup>39</sup> (Fig. 2). In these tests, the clay sample, retrieved from a core,  
97 was first consolidated under uniaxial-strain condition to the in situ vertical effective stress (point  
98 B, Fig. 2). This represents the loading on the clay as it was buried to its final depth. Then, the  
99 sample was compressed horizontally in undrained conditions; during this period, the total  
100 vertical stress was kept constant (path BCD, Fig. 2). This represents the loading that the clay

101 would undergo if it was in a shortening region, a common setting for mobile shales (Fig. 1f). The  
102 test was conducted under undrained conditions because shales have very low permeability,  
103 therefore, pore fluid could barely drain out of buried shales during shortening.

104 The clay response during undrained shortening includes two distinct phases (path BCD, Fig. 2b).  
105 First is a period of strain hardening (BC), during which deviatoric stress ( $q$ , ordinate axis in Fig.  
106 2a) increases as the clay is compressed horizontally and the shear deformation increases. During  
107 this period, the effective mean stress ( $p'$ , abscissa axis in Fig. 2a) decreases. The sample tends to  
108 compact as it is sheared, but this compaction is prevented by pore fluid that cannot escape,  
109 leading to an increase in pore pressure (shear-induced overpressure) and decrease in effective  
110 mean stress. The strain-hardening phase occurs at relatively low strains (point C in Fig. 2b).

111 The second stage consists of strain-weakening behaviour (CD, Fig. 2b), during which deviatoric  
112 stress ( $q$ ) decreases. Softening is attributed to the collapse of rock fabric or breakage of  
113 cementation/bonds, also known as *destructuration*<sup>40</sup> (sketches in Fig. 2). Destructuration entails  
114 elevated rock compression, which, in undrained conditions, translates into a significant increase  
115 in pore pressure ( $u_D$ , Fig. 2a) and decrease in effective mean stress<sup>32,41</sup>.

116 The clay reaches a state where stresses almost stop changing (point D, Fig. 2), even though the  
117 sample is still being shortened and deformed. This is the critical state, at which unlimited  
118 (plastic) shear deformation occurs without any changes in stresses or volume<sup>31,42-43</sup> (plateau, Fig.  
119 2b). The material in fact flows at the critical state, destroying the material fabric or cement  
120 (schematic boxes, Fig. 2).

121 Vane tests show that the clay flow at critical state is viscous, that is, the strain rate at critical state  
122 varies with shear stress (Fig. s6 in Supplementary Discussion 2). As such, the clay behaves as a  
123 Herschel-Bulkley material: it is solid (no flow) when shear stress is smaller than the static shear

124 strength, and when shear stress exceeds the strength, it flows at a strain rate that increases with  
125 the excess shear stress.

126 Destructuration of fabric, breaking of cement, large shear deformation, high overpressure, and  
127 plastic flow associated with the critical state tie this state to mobile shales. We therefore propose  
128 that mobile shales are at the critical state and suggest the following definition for mobile shales:  
129 “bodies of clay-rich sediment or sedimentary rock undergoing penetrative, (visco-) plastic  
130 deformation at the critical state.”

131

## 132 **Implications of a critical-state model for mobile shales**

133 *Fluidized behaviour vs grain-to-grain plasticity*

134 The critical-state model can explain not only the viscous-plastic behaviour of shales in structures  
135 such as shale diapirs, but also the fluid-like behaviour of fluidized shales in mud volcanoes. At  
136 critical state, all cements and bonds are destroyed, and the material flow is purely frictional  
137 (failure envelope has no cohesion and passes through the origin in a  $p'$ - $q$  diagram). Thus, when  
138 pore pressure increases in mud volcanoes so much as to bring the effective stresses to zero, the  
139 grains lose contact, and the shear strength becomes zero (Figs. 2a and s2 in Supplementary  
140 Discussion 2). In this case, the Herschel-Bulkley behaviour converges to a viscous-fluid model,  
141 which corresponds to the behaviour of the fluidized shale in mud volcanoes (further details in  
142 Supplementary Discussion 2 and Fig. s6).

143 The drop in effective stress leading to fluidization of shales in mud volcanoes may result from a  
144 combination of an increase in fluid pressure and a drop in total stress. One important scenario  
145 producing fluidization occurs when mobile shales rise up a fracture system below a mud

146 volcano. Total stress decreases as the material approaches the surface. This drop in total stress  
147 during rise leads to methane exsolution, elevating the pore pressure. This combination can bring  
148 effective stresses to zero, leading to the highly fluidized *ejecta* sourced from mud volcanoes.

149 *Brittle vs. ductile behaviour*

150 There is a longstanding debate concerning the relative importance of brittle and ductile  
151 behaviour in mobile shales<sup>1–3,44</sup>. Brittle behaviour is seen in a stress-strain plot with a strain-  
152 softening behaviour; i.e., residual strength at the critical state is significantly lower than peak  
153 strength (Figs. 2a–3a). Conversely, ductile behaviour exhibits strain hardening, having similar  
154 residual and peak strengths (Fig. 3). The critical-state model suggests that shales with either  
155 behaviour can reach the critical state (plateau at the end of the curves) and become mobile (Fig.  
156 3a). In Figure 2, for example, the sample reaches the critical state through brittle behaviour. A  
157 shale can behave in a brittle or ductile way, depending in part on confining stress and  
158 temperature<sup>45–47</sup> (Figs. 3a–b and s3–s4 in Supplementary Discussion 2).

159 Although deformation is ductile once the critical state is reached, any brittle structures formed  
160 during approach to the critical state may be preserved during critical-state flow to present a  
161 mixture of structural styles.

162 *Pore-fluid pressure*

163 Low velocity of mobile shales suggests overpressure is high in these shales<sup>1,3–5,8,18–19,24–29</sup>. The  
164 critical-state-model provides insight into the role that overpressure plays in shale mobilization. In  
165 principle, it is possible to reach the critical state (see the critical state line in the p'–q diagram in  
166 Fig. 2a) purely through an increase in shear, without any increase in pore pressure. However,  
167 increase in pore pressure decreases effective confining (mean) stress, making it possible to reach

168 critical state at lower shear stress. Without high overpressure, forces driving shear stress in  
169 mobile shales may not be enough to bring the shales to critical state and make them mobile. This  
170 explains the observed link between shale mobility and high pore pressures.

171 Several sources have been suggested to increase pore pressure in mobile shales, including  
172 disequilibrium compaction or generation of hydrocarbons<sup>27</sup>. The critical state model suggests  
173 shear-induced overpressure as another mechanism for increasing pore pressure in mobile shales  
174 during deformation (cf. blue curve in Fig. 2b, and Figs. s2–s4 in Supplementary Discussion 2).

175 *Degree of consolidation*

176 The critical-state concept can explain mobilization of both granular and consolidated  
177 material<sup>33–38</sup>. Consolidated or cemented shales have a higher shear strength than unconsolidated  
178 materials, particularly when they are compressed parallel to the fabric or stratification (Figs. 3c  
179 and s5 in Supplementary Discussion 2). It thus takes higher shear stress to break cements and  
180 drive these shales to the critical state. However, once this disaggregation occurs, critical-state  
181 flow can occur just as in any other shale.

182 In contrast to previous interpretations<sup>8</sup>, critical-state mechanics thus suggests that there is no  
183 depth or temperature limit on the formation of mobile shales (Figs. 3 and s2–s4 in  
184 Supplementary Discussion 2). Even if cementation has occurred, mobilization in deep shales  
185 remains possible—it just takes a higher shear stress to overcome their strength.

186 *End of shale mobility*

187 In many areas, stratal patterns on seismic data suggest that some formerly mobile shales became  
188 later inactive (Figs. 1c–e). The critical-state model provides an explanation for stabilization of  
189 formerly mobile shales. According to our model, mobile shales stop deforming when the shear

190 stress becomes smaller than the static shear strength (Fig. s6 in Supplementary Discussion 2).  
191 This may occur through either a drop in shear stress or an increase in shear strength, because in  
192 either case the shale would depart from critical-state conditions (Figs. 2–3). For example, in  
193 shales that have become mobile due to regional shortening, shear stresses may drop if shortening  
194 stops. Shear strength might increase due to dissipation of overpressure, which increases the  
195 effective mean stress and thereby the shear strength.

196 *Seismic properties*

197 The critical-state model also gives insight into seismic properties of mobile shales. First, it  
198 predicts that overpressure increases in mobile shales due to shear deformation (Figs. 2b and  
199 s2–s4 in Supplementary Discussion 2) and seismic velocity thus decreases, which affect the  
200 seismic impedance of the shales. Second, shear stiffness of a material drops significantly  
201 approaching the critical state. Therefore, our model predicts that mobile shales should have a  
202 lower S-wave velocity than immobile shales at the same porosity<sup>18–19,48</sup>. Third, although flow at  
203 the critical state destroys preexisting rock fabrics, it may create new flow fabrics<sup>2</sup>. Seismic  
204 anisotropy is therefore affected.

205 An important consideration in seismic imaging of mobile shales is whether the shales are  
206 presently mobile—that is, whether they are presently at the critical state. Once shales leave the  
207 critical state, overpressures and shale stiffness may return to normal values. However, any  
208 changes in anisotropy will remain.

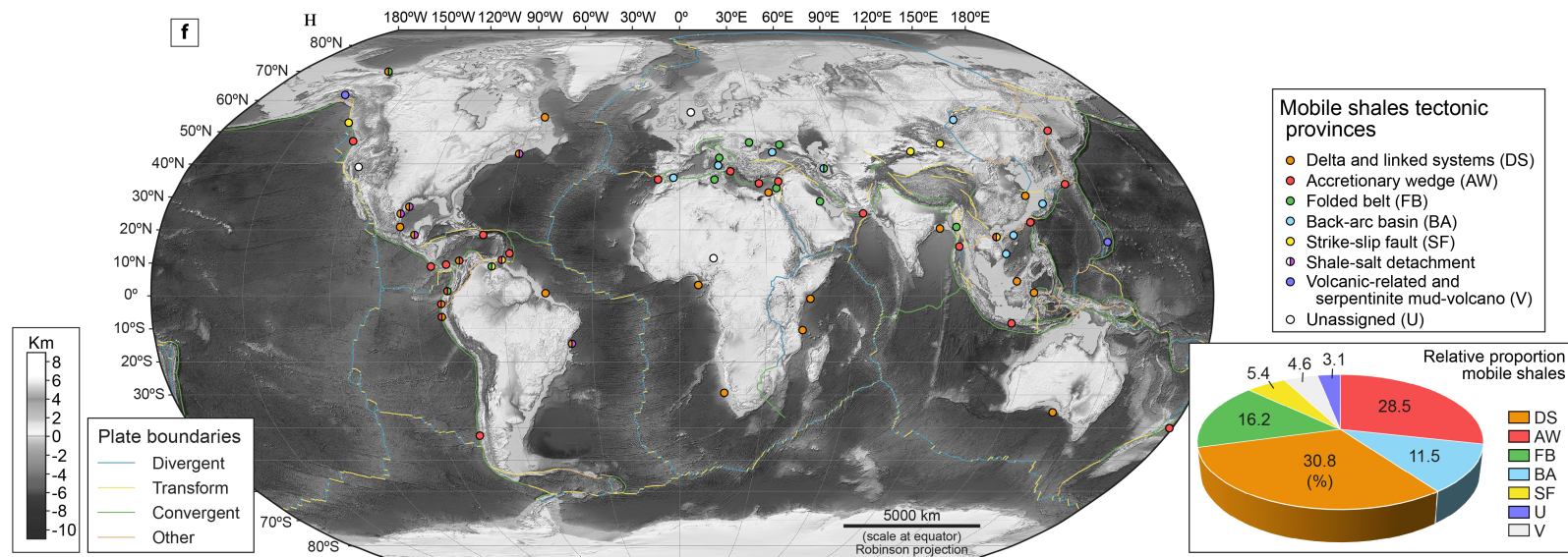
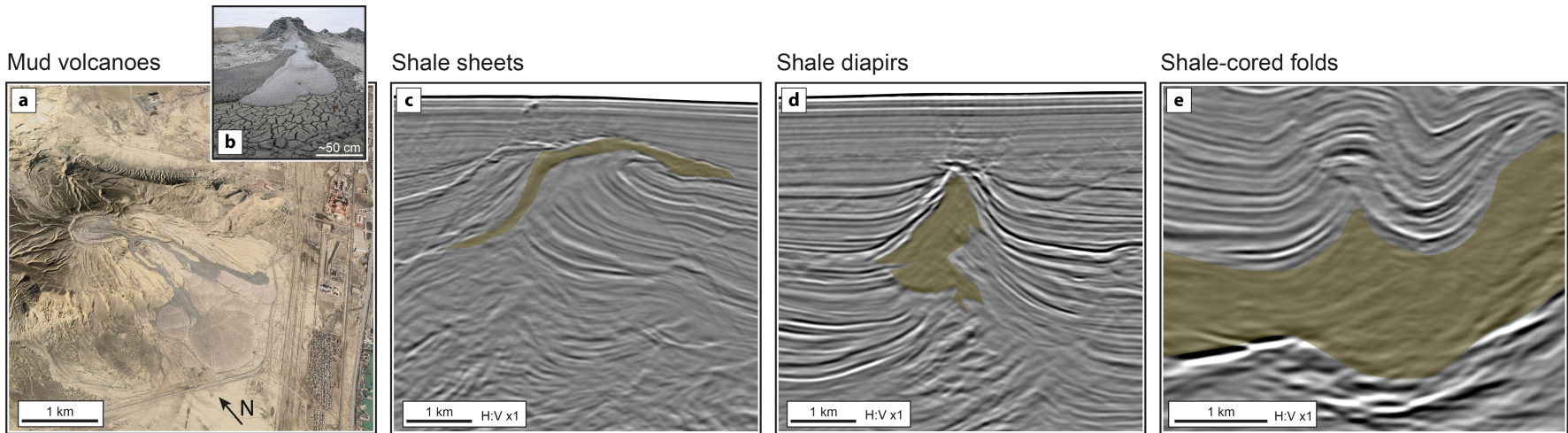
209 In conclusion, we suggest that the critical-state model is a viable hypothesis for the mechanical  
210 behaviour of mobile shales. It explains the key observations related to mobile shales, and offers  
211 many exciting prospects for future research. We look forward to seeing tests of this hypothesis as  
212 the study of mobile shales advances into the future.

213 **References**

- 214 1. Morley, C. K. & Guerin, G. Comparison of gravity-driven deformation styles and behavior associated with  
215 mobile shales and salt. *Tectonics* **15**, 1154-1170 (1996).
- 216 2. Morley, C. K., von Hagke, C., Hansberry, R. L., Collins, A. S., Kanitpanyacharoen, W. & King, R. Review of  
217 major shale-dominated detachment and thrust characteristics in the diagenetic zone: Part I, meso- and macro-  
218scopic scale. *Earth Sci. Rev.* **173**, 168-228 (2017).
- 219 3. Wood, L. in *Shale Tectonics* (ed. Wood, L.) 1-4 (AAPG Mem. **93**, 2010).
- 220 4. Morley, C. K., Tingay, M., Hillis, R. & King, R. Relationship between structural style, overpressures, and  
221 modern stress, Baram Delta Province, northwest Borneo. *J. Geophys. Res.* **113**, B09410 (2008).
- 222 5. Duerto, L. & McClay, K. Role of the shale tectonics on the evolution of the Eastern Venezuelan Cenozoic thrust  
223 and fold belt. *Mar Pet. Geol.* **28**, 81-108 (2011).
- 224 6. Aplin, A. C., Fleet, A. J. & Macquaker, J. H. S. in *Muds and Mudstones: Physical and Fluid Flow Properties*  
225 (eds. Aplin, A. C., et al.) 1-8 (*Geol. Soc. Spec. Publ.* **158**, 1999).
- 226 7. Peltonen, C., Marcussen, Ø., Bjørlykke, K. & Jahren, J. Clay mineral diagenesis and quartz cementation in  
227 mudstones: the effects of smectite to illite reaction on rock properties. *Mar. Pet. Geol.* **26**, 887-898 (2009).
- 228 8. Day-Stirrat, R. J., McDonnell, A. & Wood, L. J. in *Shale Tectonics* (ed. Wood, L.) 5-27 (AAPG Mem. **93**, 2010).
- 229 9. Milkov, A. V. Worldwide distribution of submarine mud volcanoes and associated gas hydrates. *Mar. Geol.* **167**,  
230 29-42 (2000).
- 231 10. Dimitrov, L. I. Mud volcanoes—the most important pathway for degassing deeply buried sediments. *Earth Sci.*  
232 *Rev.* **59**, 49-76 (2002).
- 233 11. Kopf, A. Significance of mud volcanism. *Rev. Geophys.* **40**, 1005 (2002).
- 234 12. Alizadeh, A. A., Guliev, I. S., Dadashov, F. H. & Rahmanov, R. R. *Atlas of the World Mud Volcanoes* (Nafta-  
235 Press, Baku, 2015).
- 236 13. Mazzini, A. & Etiope, G. Mud volcanism: An updated review. *Earth Sci. Rev.* **168**, 81-112 (2017).
- 237 14. Kerr, P. F., Drew, I. M. & Richardson, D. S. Mud volcano clay, Trinidad, West Indies. *AAPG Bull.* **54**, 2101-  
238 2110 (1970).
- 239 15. Williams, P. R., Piagram, C. J. & Dow, D. B. Melange production and the importance of shale diapirism in  
240 accretionary terrains. *Nature* **309**, 145-146 (1984).
- 241 16. Petley, D. N. in *Muds and Mudstones: Physical and Fluid Flow Properties* (eds. Aplin, A. C., et al.) 61-71  
242 (*Geol. Soc. Spec. Publ.* **158**, 1999).
- 243 17. Kopf, A. J., Clennell, B. & Brown, K. M. in *Mud Volcanoes, Geodynamics and Seismicity* (eds. Martinelli, G. &  
244 Panahi, B.) 263-283 (Springer, 2005).
- 245 18. Henry, M., Pentilla, M. & Hoyer, D. in *Shale Tectonics* (ed. Wood, L.) 63-78 (AAPG Mem. **93**, 2010).
- 246 19. Lupi, M., Saenger, E. H., Fuchs, F. & Miller, S. A., 2013. Lusi mud eruption triggered by geometric focusing of  
247 seismic waves. *Nat. Geosci.* **6**, 642-688 (2013).
- 248 20. Pralle, N., Külzer, M. & Gudehus, G. in *Subsurface Sediment Mobilization* (eds. Van Rensbergen, P., et al.) 159-  
249 171 (*Geol. Soc. Spec. Publ.* **216**, 2003).
- 250 21. Tran, A., Rudolph, M. L. & Manga, M. Bubble mobility in mud and magmatic volcanoes. *J. Volcanol.*  
251 *Geotherm. Res.* **294**, 11-24 (2015).
- 252 22. Mazzini, A. et al. Explosive mud volcano eruptions and rafting of mud breccia blocks. *Earth Planet. Sci. Lett.*  
253 **555**, 116699 (2021).
- 254 23. Haghighat, E., Rassouli, F. S., Zoback, M. D. & Juanes, R. A viscoplastic model of creep in shale. *Geophys.* **85**,  
255 MR155-MR166 (2020).
- 256 24. Roberts, K. S., Davies, R. J. & Stewart, S. A. Structure of exhumed mud volcano feeder complexes, Azerbaijan.  
257 *Basin Res.* **22**, 439-451 (2010).
- 258 25. Soto, J. I., Fernández-Ibáñez, F., Talukder, A. R. & Martínez-García, P. in *Shale Tectonics* (ed. Wood, L.) 119-  
259 144 (AAPG Mem. **93**, 2010).
- 260 26. Soto, J. I., Hudec, M. R., Mondol, N. H. & Heidari, M. Shale transformations and physical properties—  
261 implications for seismic expression of mobile shales. *Earth Sci. Rev.* (under review).
- 262 27. Osborne, M. J. & Swarbrick, R. E. Mechanisms for generating overpressure in sedimentary basins: A  
263 reevaluation. *AAPG Bull.* **81**, 1023-1041 (1997).
- 264 28. Inan, S. et al. Deep petroleum occurrences in the Lower Kura Depression, South Caspian Basin, Azerbaijan: an  
265 organic geochemical and basin modelling study. *Mar. Pet. Geol.* **14**, 731-762 (1997).

- 266 29. Planke, S. et al. Mud and fluid migration in active mud volcanoes in Azerbaijan. *Geo-Mar. Lett.* **23**, 258-268  
267 (2003).
- 268 30. Sautkin, A. et al. Mud volcanoes in the Alboran Sea: evidence from micropaleontological and geophysical data.  
269 *Mar. Geol.* **195**, 237-261 (2003).
- 270 31. Roscoe, K. H. & Burland, J. B. in *Engineering Plasticity* (eds. Heyman, J. & Leckie, F. A.) 535-609 (Cambridge  
271 University Press, Cambridge, 1968).
- 272 32. Schofield, A. N. & Wroth, C. P. *Critical State Soil Mechanics* (McGraw-Hill, London, 1968).
- 273 33. Steiger, R. P. & Leung, P. K. Quantitative determination of the mechanical properties of shale. *SPE Drill.  
274 Complet.* **7**, 181-185 (1992).
- 275 34. Horsrud, P., Sønstebo, E. F. & Bøe, R. Mechanical and petrophysical properties of North Sea shales. *Int. J. Rock  
276 Mech. Min. Sci.* **35**, 1009-1020 (1998).
- 277 35. Ewy, R., Dirkzwager, J. & Bovberg, C. Claystone porosity and mechanical behavior vs. geologic burial stress.  
278 *Mar. Pet. Geol.* **121**, 104563 (2020).
- 279 36. Albertz, M. & Sanz, P. F. Critical state finite element models of contractional fault-related folding: Part 2.  
280 Mechanical analysis. *Tectonophysics* **576-577**, 150-170 (2012).
- 281 37. Obradors-Prats, J., Rouainia, M., Aplin, A. C. & Crook, A. J. L. Hydro-mechanical modelling of stress, pore  
282 pressure and porosity evolution in fold-and-thrust belt systems. *J. Geophys. Res. B: Solid Earth* **122**, 9383-9403  
283 (2017).
- 284 38. Obradors-Prats, J., Rouainia, M., Aplin, A. C. & Crook, A. J. L. A diagenesis model for geomechanical  
285 simulations: formulation and implications for pore pressure and development of geological structures. *J.  
286 Geophys. Res. B: Solid Earth* **124**, 4452-4472 (2019).
- 287 39. Westerberg, B. *Lerors Mekaniska Egenskaper: Experimentell Bestämning och Kvalitativ Modellering med  
288 Tillämpning på Lera från Norrköping* [Licenciate thesis, Luleå University of Technology, Sweden] (1995).
- 289 40. Rouainia, M. & Muir Wood, D. A kinematic hardening constitutive model for natural clays with loss of  
290 structure. *Géotechnique* **50**, 153-164 (2000).
- 291 41. Lambe, T. W. & Whitman, R. V. *Soil Mechanics* (SI Version, 2<sup>nd</sup> ed) (John Wiley & Sons, New York, 1979).
- 292 42. Atkinson, J. H. & Bransby, P. L. *The Mechanics of Soils: An Introduction to Critical State Soil Mechanics*  
293 (McGraw-Hill, London, 1978).
- 294 43. Muir Wood, D. *Soil Behaviour and Critical State Soil Mechanics* (Cambridge University Press, Cambridge,  
295 1991).
- 296 44. Restrepo-Pace, P. A. in *Passive Margins: Tectonics, Sedimentation and Magmatism* (ed. McClay, K. R. &  
297 Hammerstein, J. A.) 193-204 (*Geol. Soc. Spec. Publ.* **476**, 2020).
- 298 45. Rybacki, E., Meier, T. & Dresen, G. What controls the mechanical properties of shale rocks? – Part II:  
299 Brittleness. *J. Pet. Sci. Eng.* **144**, 39-58 (2016).
- 300 46. Wang, S. et al. A universal method for quantitatively evaluating rock brittle-ductile transition behaviors. *J. Pet.  
301 Sci. Technol.* **195**, 107774 (2020).
- 302 47. Masri, M., Sibai, M., Shao, J. F. & Mainguy, M. Experimental investigation of the effect of temperature on the  
303 mechanical behavior of Tournemire shale. *Int. J. Rock Mech. Min. Sci.* **70**, 185-191 (2014).
- 304 48. Couzens-Schultz, B. A. & Azbel, K. Predicting pore pressure in active fold-thrust systems: An empirical model  
305 for the deepwater Sabah foldbelt. *J. Struct. Geol.* **69**, 465-480 (2014).
- 306 49. Hovland, M., Imbert, P. & Ho, S. Fluid venting system website. <https://www.fluid-venting-system.org> (accessed  
307 in June 2020).
- 308 50. Islam, M. A. & Skalle, P. An experimental investigation of shale mechanical properties through drained and  
309 undrained test mechanisms. *Rock Mech. Rock Eng.* **46**, 1391-1413 (2013).
- 310
- 311

312 **Figures**

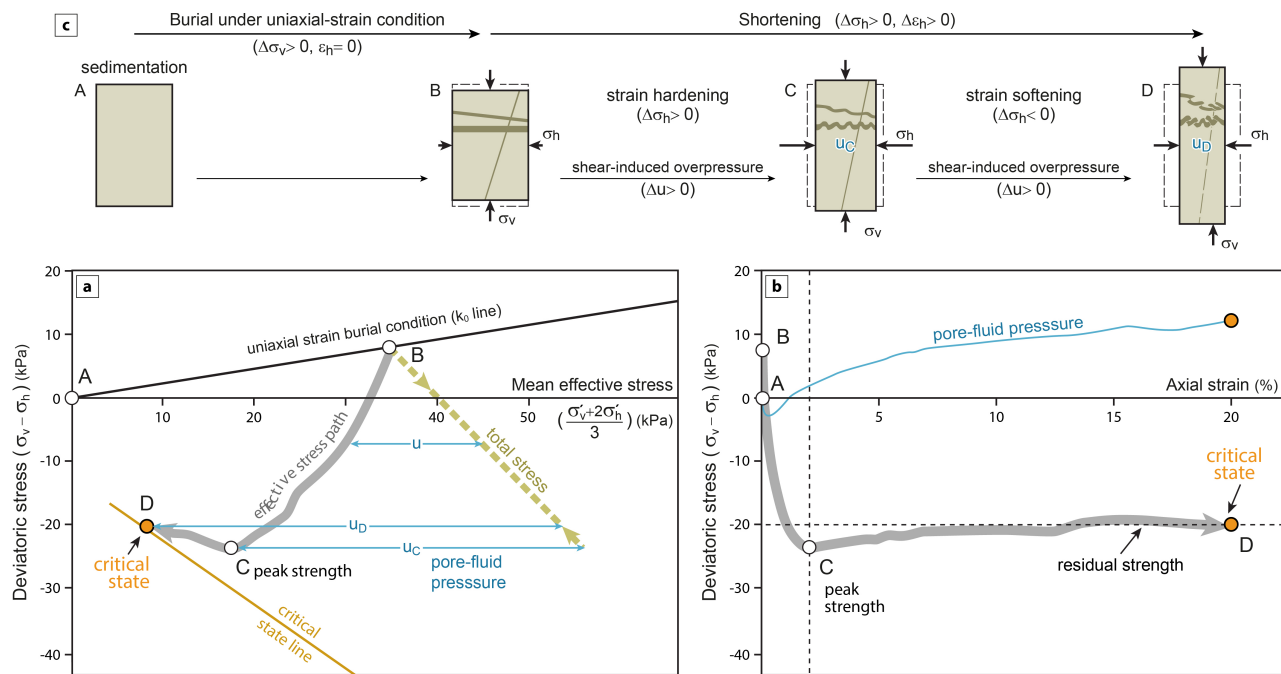


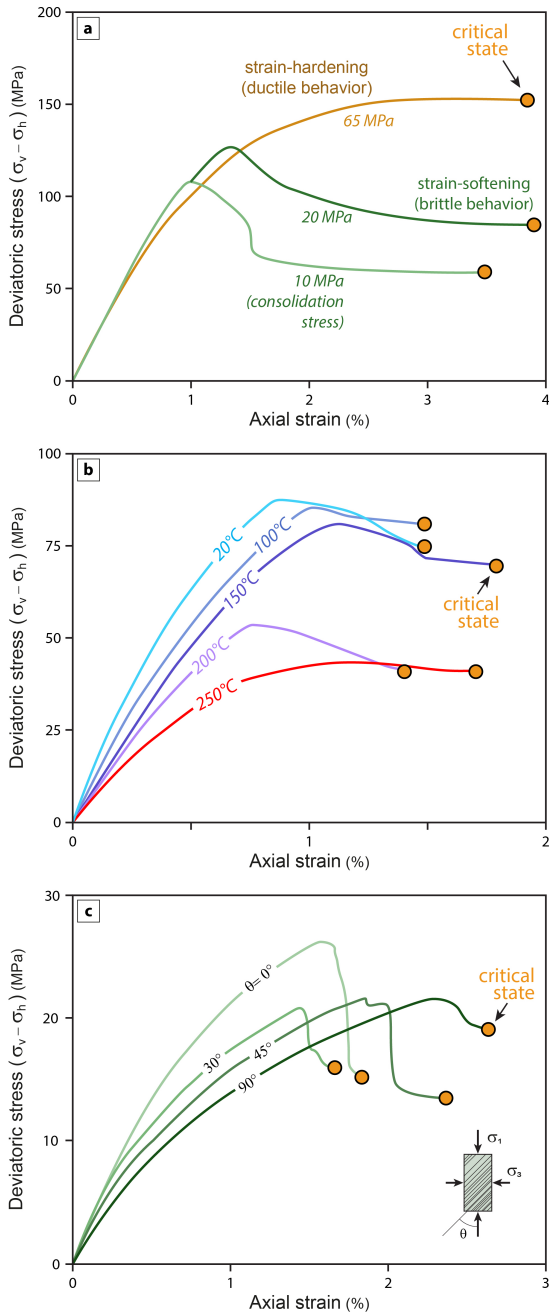
313

314 **Fig. 1** (legend in next page)

315 ↑ **Fig. 1 | Structures formed by mobile shales.** **a**, Garadagh mud volcano in onshore Azerbaijan (40.24°N  
 316 and 49.51°E). **b**, Gryphon structure within the Dashgil mud volcano<sup>49</sup> in onshore Azerbaijan (39.99°N  
 317 and 49.47°E). **c–e**, Buried mobile shales, as seen in seismic profiles (offshore, north-western Gulf of  
 318 Mexico): **c**, shale sheet; **d**, shale diapir, and **e**, shale-cored folds. Seismic images extracted from a 3D  
 319 depth seismic cube (seismic data courtesy of PGS). **f**, Global distribution of mobile-shale structures over  
 320 plate-tectonic map of Earth. Surface-elevation model and complete details of compilation in  
 321 Supplementary Discussion 1 (Fig. s1 and Table s1). Map plotted using Robinson projection. Inset pie  
 322 diagram shows relative proportion (in %) of mobile shales according to their tectonic setting (for total  
 323 population of 65 regions; Supplementary Table s1).

324  
 325





339

340 **Fig. 3 | Experimental stress-strain curves and critical-state conditions in shales.** **a**, Mudstone samples  
 341 from Kuqa Depression (Tarim Basin, China) deformed at different consolidation stresses<sup>46</sup>. Brittle  
 342 behaviour characterized by strain-softening (experiments at consolidation stresses of 10 and 20 MPa),  
 343 ductile behaviour showing no difference between peak and residual strengths (consolidation stress of 65  
 344 MPa). Tests with compression perpendicular to bedding. **b**, Stress-strain curves for Tournemire shale  
 345 (Massif Central, France) deformed at different temperatures<sup>47</sup>. Tests under constant consolidation stress  
 346 (20 MPa) and compression perpendicular to bedding. **c**, Stress-strain curves for Pierre-1 shale (USA)  
 347 deformed with different orientations ( $\theta$ ) of bedding<sup>509</sup>. Tests under constant consolidation stress (25  
 348 MPa). Other symbols like in Fig. 2. Detailed information about these experimental tests and about shale  
 349 samples in Supplementary Discussion 2 (Tables s2–s3). Additional experiments documenting how  
 350 confining pressure, temperature, and fabric anisotropy affect geomechanical behaviour of shales in Figs.  
 351 s3, s4, and s5, respectively (Supplementary Discussion 2).

352 **Acknowledgements**

353 We thank Nancy Cottington for initial figure drafting. The project was funded by the Applied Geodynamics  
354 Laboratory (AGL) Industrial Associates program, comprising the following companies: Anadarko, Aramco Services,  
355 BHP Billiton, BP, CGG, Chevron, Condor, Ecopetrol, EMGS, ENI, ExxonMobil, Hess, Ion-GXT, Midland Valley,  
356 Murphy, Nexen USA, Noble, Petrobras, Petronas, PGS, Repsol, Rockfield, Shell, Spectrum, Equinor, Stone Energy,  
357 TGS, Total, WesternGeco, and Woodside (<http://www.beg.utexas.edu/agl/sponsors>). Publication authorized by the  
358 Director, Bureau of Economic Geology, The University of Texas at Austin.

359 **Author contributions**

360 J.I.S., M.H. and M.R.H. conceived and designed the study, co-writing the paper.

361 **Competing interests**

362 The authors declare no competing interests.

363 **Additional information**

364 **Supplementary Discussion 1.** Global distribution of mobile-shale structures

365 Figure s1 (Global distribution of the mobile-shale structures according to tectonic setting)

366 Table s1 (List of regions with mobile shales)

367 Supplementary references for Fig. s1

368

369 **Supplementary Discussion 2.** Composition and geomechanical-test conditions in shales

370 Table s2 (Composition and geomechanical-test conditions of various shales compiled for this study)

371 Table s3 (Ternary diagrams for classification of shales)

372 Figure s2 (Stress paths and stress-strain curves for shales—Supplementary to Fig. 2)

373 Figure s3 (Stress-strain curves for shales under different confining pressures—Supplementary to Fig. 3a)

374 Figure s4 (Stress-strain curves for shales under different temperature conditions—Supplementary to Fig. 3b)

375 Figure s5 (Stress-strain curves for shales depending on orientation of fabric—Supplementary to Fig. 3c)

376 Figure s6 (Shear strength of London Clay measured using Vane test)

377 Supplementary references for Tables s2–s3 and Figures s2–s6

## Supplementary Files

This is a list of supplementary files associated with this preprint. Click to download.

- [SupplementaryMaterialSotoetalv6revisedall.pdf](#)